10.1515/astro-2017-0169

Baltic Astronomy, vol. 23, 9–26, 2014

CORRELATIONS IN RELAXED CLUSTERS OF GALAXIES

Iu. Babyk[1,2,3] and A. Del Popolo[4,5]

[1] *Main Astronomical Observatory, NAS of Ukraine, Zabolotnogo str., 27, 03650, Kyiv, Ukraine*

[2] *Dublin Institute for Advanced Studies, 31 Fitzwilliam Place, Dublin 2, Ireland*

[3] *Dublin City University, Dublin 9, Ireland*

[4] *Dipartimento di Fisica e Astronomia, Universitá di Catania, Viale Andrea Doria 6, 95125 Catania, Italy*

[5] *International Institute of Physics, Universidade Federal do Rio Grande do Norte, 59012-970 Natal, Brazil*

Received: 2014 February 3; accepted: 2014 March 15

Abstract. The correlations among different quantities in galaxy clusters, observed by Newman et al. (2013a,b), are investigated. We find an anti-correlation among the slope α, the effective radius, $R_{\rm e}$, and a correlation among the core radius $r$core and Re. Moreover, the mass inside 100 kpc (mainly dark matter) is correlated with the mass inside 5 kpc (mainly baryons). The listed correlations can be understood in a two phase formation model: the first dissipative phase forming the brightest cluster galaxies, and the second dissipationless phase, in which the inner density profile is flattened by the interaction of baryonic clumps and the dark matter halo through dynamical friction.

Key words: cosmology: theory, large-scale structure of Universe – dark matter – galaxies: clusters, formation

1. INTRODUCTION

The Λ cold dark matter (ΛCDM) model is successful in explaining a large range of data on cosmological scales, like the baryonic acoustic oscillation features in the matter power spectrum (Percival et al. 2010) and the anisotropy and polarization spectrum of the cosmic microwave background radiation (Komatsu et al. 2011; Del Popolo 2007, 2013). Despite a long list of successes of the ΛCDM model, it suffers some tension at scales from a few kpc to tens of pc(Del Popolo & Gambera 1997; Del Popolo et al. 2014). The ΛCDM model also suffers from other drawbacks, like the "cosmological constant problem" (Weinberg 1989), and the "cosmic coincidence problem". The first one is connected to the fact that most quantum field theories predict a huge cosmological constant from the energy of the quantum vacuum, which is more than 100 orders of magnitude too large (see Weinberg 1989; Astashenok & Del Popolo 2012; Martin 2012). Moreover, in general the open question remains if dark energy is a cosmological constant or a

dynamical component of the universe (see Cremenelli et al. 2009).

A fundamental prediction of the cold dark matter (CDM) paradigm is the structure of dark matter (DM) haloes that have a central density cusp, characterized by $\rho_{\rm DM} \simeq r^{\alpha}$ (Navarro, Frenk & White 1996, 1997 (hereafter NFW), Moore et al. 1998, Navarro et al. 2004, 2010). The debated value of α ranges from $\alpha = -1.5$ (Moore et al. 1998) to $\alpha = -0.8$ (Stadel et al. 2009).

Observations of galaxies which are DM dominated (e.g., dwarf spferoidals (dSphs), dwarf spirals, low-surface-brightness galaxies (LSBs)), are at odds with simulations, finding core-like density profiles (e.g., Flores & Primack 1994; Moore 1994; Oh et al. 2010; Del Popolo & Hiotelis 2014). In dSphs and ellipticals, the determination of the DM mass profile is challenging, because of the small dynamic range of observations, the degeneracies related to the mass probes used in the profile determination (e.g., velocity anisotropy), and the difficulty in disentangling baryons and DM (see Del Popolo 2014, section "Dark matter distribution"). The quoted problems can be overcome in clusters of galaxies, since clusters have properties that can be understood and interpreted in a simpler fashion than galaxy rotation curves. Several observational probes (e.g., X-ray emission from intracluster plasma, gravitational lensing) furnish an accurate measure of mass (e.g. Babyk & Vavilova 2014; Babyk et al. 2012a,b,c; Allen et al. 2011; Kneib & Natarajan 2011).

In recent years, studies of clusters of galaxies showed that the DM profiles are flatter than those obtained in the simulations (Sand et al. 2002, 2004, 2008 (Sa02; Sa04, Sa08); Newman et al. 2009, 2011, 2013a,b (N09, N11, N13a,b); Babyk et al. 2012a), within a radius of $\simeq 30$ kpc, typical of the radius of brightest cluster galaxies (BCG). Moreover, the DM profile is characterized by a variation of the slope, $\alpha = -d\log\rho_{DM}/dr$, from cluster to cluster, and the variation correlates with the BCG properties. A similar scatter is observed in galaxies. The quoted discrepancy among the results of dissipationless simulations and observations is interpreted in terms of the fact that dissipationless simulations do not take into account baryons that are of fundamental importance in the inner parts of galaxies and clusters (see N13b). The quoted discrepancy is reduced or eliminated both in galaxies and clusters of galaxies, when baryons are taken into account by means of smooth particle hydrodynamics (SPH) simulations or by semi-analytical models (El-Zant et al. 2001, 2004; Del Popolo & Kroupa (2009); Del Popolo 2009 (DP09), Del Popolo 2010 (DP10), Del Popolo 2011 (DP11), Del Popolo 2012a,b (DP12a,b); Cardone & Del Popolo 2012; Del Popolo, Cardone, Belvedere 2013; Cole et al. 2011; Cardone et al. 2011; Martizzi et al. 2012a).

In DP12a, the model introduced in DP09 was used to study how baryonic physics influences the shape of the density profiles of clusters. It was shown that the presence of baryons in the inner 10 kpc of the structure modifies the inner profile. Also, the correlation among the inner baryon content (mass of the BCG) and the slope of the density profile has been found.

Meanwhile, N13b used a larger sample[1] than the samples used in previous studies, to obtain a joint measurement of the stellar mass scale. Among the other results, they found correlations between the slope of the inner part of the DM density profile and some BCG structure parameters.

[1]The seven clusters constituting the sample are: MS2137, A963, A383, A611, A2537, A2667, A2390.

N13a presented the results obtained with the strong and weak lensing, and stellar kinematics for the relaxed galaxy clusters MS2137, A963, A2537, A2667, A2390, A611, and A383 at $z = 0.19 - 0.31$, and having masses in the range $M_{200} = 0.4 - 2 \times 10^{15} M_{\odot}$. The total radial density profiles were studied both for DM and baryonic matter on the scales $\simeq 3 - 3000$ kpc. The data obtained by N13a have a better quality than those presented in previous papers (e.g., N09, N11). Weak lensing was measured using the deep multicolor imaging technique, using the Subaru telescope and the multiply imaged sources with the Hubble Space Telescope (25 strongly lensed sources, of which 21 have spectroscopic redshifts). The stellar kinematic profiles were obtained with the Keck telescopes. The X-ray data were taken from the *Chandra* archive, and the CIAO tools were used to remove the point sources.

A611, A383, MS2137, A963 and A2667 are typically relaxed clusters. The X-ray emission is symmetric, regular and well aligned with the BCG. The X-ray centroid is a few kpc from the BCG. The redshifts of A383, A611 and A2667 are consistent with a unimodal distribution with the BCG at rest in the potential of the clusters. The X-ray emission in A2390 is more complicated, showing an extension in the northwest direction, on a scale of $\simeq 200$ kpc. On larger scales the galaxy and X-ray distribution are regular, the galaxies of the cluster have a unimodal velocity distribution, centered on the BCG. A2537 is the most disturbed cluster in the sample. Nevertheless the X-ray emission is symmetric and regular, it is centered at north of the BCG. The second mass concentration could be present, judging from the arcs curvature. The distribution of the cluster galaxy velocities is bimodal. Probably, A2537 is not a fully relaxed cluster.

In order to infer the cluster mass distribution and density profile, the cluster mass was modeled with a DM halo and a generalized NFW profile. The stars in the BCG and the mass in the other galaxies present in the cluster were modeled with a dPIE profile (Eq. 1 in N13a). Mass models were obtained from the data using the Lenstool code (Jullo et al. 2007), modified to incorporate the constraints coming from the weak lensing and stellar kinematics.

N13a,b presented an intuitive interpretation of the results and correlations found in the observations, proposing a "physical picture" based on previous theoretical results (e.g., El-Zant et al. 2001, 2004; DP09; DP12a). The "physical picture" proposed by N13a,b, is based on the first dissipative phase in which the BCG forms, and the second dissipationless phase in which DF between the baryon clumps (collapsing to the center of the proto-structure) and the DM halo reduces the central DM density.

It would be interesting to see if the quoted correlations can be re-obtained using a theoretical model, to understand what produces them, and eventually to confirm if the "physical picture" proposed by N13a,b is consistent. To this aim, we use the observations and the new data published in N13a,b and the model of DP09 and DP12a to study the density profiles and correlations.

2. SUMMARY OF THE MODEL

The model used in the present paper is that described in DP09 and DP12a,b to which we refer readers for details. Here we give a summary of the model.

DP09 is an improved spherical infall model (SIM) which differs from previous SIMs because it simultaneously takes into account the following effects that in

previous SIMs were taken into account separately: random angular momentum (e.g., Williams et al. 2004), DF of stellar/DM clumps against the background halo (e.g., El-Zant et al. 2001; Romano-Diaz et al. 2008) and adiabatic contraction (e.g., Blumenthal et al. 1986; Gnedin et al. 2004; Gustafsson et al. 2006).

Following Gunn & Gott (1972), the protostructure is considered as being formed by concentric shells expanding with the Hubble flow. Starting from an initial comoving radius x_i, each shell expands to a maximum radius, x_m, usually termed turn-around radius, $r_{\rm ta}$, and then it collapses giving rise to a "virialized" structure, when non-linear processes in the collapse phase convert the kinetic energy into random motions.

The final density is given by (Gunn 1977; Fillmore & Goldreich 1984)

$$\rho(x) = \frac{\rho_{\rm ta}(x_m)}{f(x_i)^3}\left[1 + \frac{d\ln f(x_i)}{d\ln x_m(xi)}\right]^{-1} \tag{1}$$

where the term $f(x_i) = x/x_m(x_i)$ is the so-called collapse factor (see Eq. A18, DP09).

In the original secondary infall model (SIM) of Gunn & Gott (1972), the collapse was radial and did not take into consideration the angular momentum, which originates from tidal interaction of the proto-structure with the neighbors (Peebles 1969; Schaefer 2009). This "ordered" angular momentum is obtained integrating the torque over time on each mass shell (e.g., Ryden 1988, Eq. 35).

It is usual to express the total angular momentum in terms of a dimensionless quantity, the spin parameter λ:

$$\lambda = \frac{L|E|^{1/2}}{GM^{5/2}} = \frac{L}{2G^{1/2}M^{3/2}R^{1/2}}, \tag{2}$$

(Peebles 1969) where E is the halo's binding energy, L is the angular momentum.

A "random" angular momentum, j, is also present in haloes, and is generated by random velocities (Ryden & Gunn 1987). It can be taken into account by assigning an angular momentum at turn-around (e.g., Hiotelis 2002; Ascasibar et al. 2004),

$$j = j_* \propto \sqrt{GMx_m}, \tag{3}$$

which can also be expressed in terms of the eccentricity ratio $e_0 = \left(\frac{r_{\rm min}}{r_{\rm max}}\right)_0$, $r_{\rm max}$ and $r_{\rm min}$ being the apocentric and pericentric radii, respectively. N-body simulations show that $< \frac{r_{\rm min}}{r_{\rm max}} > \simeq 0.2$ in virialized haloes (Avila-Reese et al. 1998). Since moving to the turn-around radius, $r_{\rm ta}$, the particle orbits are more radial, one needs to use a correction as shown by Ascasibar et al. (2004)

$$e(r_{\rm max}) \simeq 0.8(r_{\rm max}/r_{\rm ta})^{0.1} \tag{4}$$

for $r_{\rm max} < 0.1r_{\rm ta}$. Then angular momentum can be taken into account using the previous approach (Avila-Reese et al. 1998) with the Ascasibar et al. correction.

The deceleration term connected to DF was introduced in the equation of motion (Eq. A14 in DP09). The DF coefficient was obtained similarly to Antonuccio-Delogu & Colafrancesco (1994) (see also Appendix D of DP09).

The adiabatic contraction (AC) of DM, produced by the collapse of baryons, was taken into account as follows. The protostructure is made of baryons and DM,

baryonic fraction $F_b = M_b/M_{500} << 1$, and DM fraction $1 - F_b$[2]. Baryons cool and collapse towards the structure center giving rise to a distribution $M_b(r)$. DM is compressed, and particles located initially at r_i move to a new position

$$r\,[M_b(r) + M_{\rm dm}(r)] = r_i M_i(r_i) \tag{5}$$

(Blumenthal et al. 1986), here $M_i(r_i)$ is the total mass at initial time and $M_{\rm dm}$ is the final distribution of DM. One then assumes that baryons and DM have the same initial distribution (Mo et al. 1998; Cardone & Sereno 2005; Treu & Koopmans 2002; Keeton 2001), and that the final baryon distribution is a Hernquist configuration (Rix et al. 1997; Keeton 2001; Treu & Koopmans 2002). If particle orbits do not cross, we have

$$M_{\rm dm}(r) = (1 - F_b) M_i(r_i) \tag{6}$$

Once $M_i(r_i)$ and $M_b(r)$ are given, Eqs. (5) and (6) can be solved to find the final halo distribution. The previous model can be improved assuming that

$$M(\bar{r})r = \text{const.} \tag{7}$$

(Gnedin et al. 2004) and the product of the mass in the orbit-averaged radius $\bar{r}$ with radius conserves. The quantity

$$\bar{r} = \frac{2}{T_r} \int_{r_{\rm min}}^{r_{\rm max}} r\,\frac{dr}{v_r}, \tag{8}$$

is the orbit-averaged radius, and T_r is the radial period.

In the late phase of structure formation, baryon density increases and this produces a sort of coupling among DM and baryons (Klypin et al. 2001, 2002), with a consequent exchange of angular momentum among baryons and DM (see DP12a, Eqs. 11-14).

The baryon fraction adopted was that obtained by Giodini et al. (2009), $f_B = f_{500}^{\rm stars+gas} = M_{500}^{\rm stars+gas}/M_{500}$[3]

In DP12a, we studied the mass/density profiles of A611, A383 (also studied in this paper), MACS J1423 and RX J1133. We also studied the existence of (a) the correlation among the inner slope and the ratio of baryonic to total mass; (b) the correlation among the total mass and the baryonic mass in the inner 10 kpc; (c) the correlation among the inner slope and the ratio of the baryonic mass in 10 kpc and the total mass. In the present paper, we studied the correlation among the inner slope and the effective radius, and the correlation among the mass in 100 kpc, which is mainly DM, and that in 5 kpc, which mainly consists of baryons. In the present paper, we investigated more clusters, including MS2137, A963, A2537, A2667, A2390, which were not studied in DO12a.

[2] M_{500} is the mass enclosed in the radius R_{500} within which the density is $500\,\rho_c$, here ρ_c is the critical density. The total baryonic mass, M_b, is given by the sum of the gas mass, $M_{\rm gas}$, and the mass in stars, M_*.

[3] In this paper the masses, M_{200} and $M_{\rm vir}$, are converted to M_{500} following White (2001), Hu & Kravtsov (2 003), Lukic et al. (2009), Hiotelis & Del Popolo (2006, 2013). The quoted Giodini et al. (2009) result was obtained using 118 groups and clusters, 91 of which were selected from the COSMOS 2 deg^2 survey in the redshift range 0.1–1.0. The data were fitted using the method of the weighted least squares with intrinsic scatter (WLSS) (Pratt et al. 2006).

Table 1. Parameters of the clusters. Column (1): the name of the cluster; (2) the M_{200} mass given in N13a; (3) the baryon fraction obtained from Giodini et al. (2009) using the previous M_{200} masses; (4) the slope α obtained by N13b modeling the profile with a gNFW model; (5) as the previous column but the profiles were obtained using the model of the present paper; (6) the core radius (in kpc) obtained by N13b modeling profile with a cNFW model; (7) as the previous column but the profile is obtained using the model of the present paper; (8) the BCG mass and errors obtained in N13a; (9) as the previous column but using the model of the present paper; (10) the value of j.

Cluster	$\log\frac{M_{200}}{M_\odot}$	$f_{\rm B}$	$\alpha^{\rm N13b}_{\rm gNFW}$	$\alpha^{\rm our}_{\rm gNFW}$	$\log r(\rm core)^{\rm N13b}_{\rm cNFW}$	$\log r(\rm core)^{\rm our}_{\rm cNFW}$	$\frac{M_{\rm BCG}}{10^{11}M_\odot}$	$\frac{M_{\rm BCG}}{10^{11}M_\odot}$	j
MS2137	14.56	0.130	0.65	0.66	0.45	0.44	6.56	6.6	$1j_*$
A963	14.61	0.131	0.50	0.51	0.87	0.86	10.65	10.7	$1.4j_*$
A383	14.82	0.137	0.37	0.37	0.37	0.37	9.18	9.2	$1.75j_*$
A611	14.92	0.140	0.79	0.79	0.47	0.47	12.25	12.3	$j_*/1.5$
A2537	15.12	0.146	0.23	0.22	1.67	1.68	13.60	13.5	$2.1j_*$
A2667	15.16	0.147	0.42	0.41	1.29	1.30	7.94	7.8	$1.6j_*$
A2390	15.34	0.153	0.82	0.82	0.30	0.30	5.26	5.3	$j_*/1.4$

The density profiles produced by the quoted model are in agreement with those of previous studies (e.g., El-Zant et al. 2001, 2004; Romano-Diaz et al. 2008; Cole et al. 2011).

3. RESULTS

In DP12a and DP12b the inner slope and its scatter were studied in the case of clusters and galaxies, respectively. It was shown that the role of environment (see also Del Popolo & Cardone 2012), and the consequent structural differences among structures give rise to galaxies and clusters with different inner slope. It was shown how different baryonic fraction, and angular momentum changes the profile of the structure: the structures, having larger baryon content (especially in the central region) and larger angular momentum, have flatter inner profiles. Similarly to DP12a, we use the model, previously described, to obtain the mass profiles of the seven clusters studied in N13a, N13b.

The precise density profile determination is challenging, especially in the case when one wants to separate the baryonic and dark matter components. A method combining different techniques like weak and strong lensing with measures of stellar kinematics can give better results. In the literature, the previous technique is used in a few papers (e.g., Sa02; Sa04, Sa08; N09; N11; N13a,b).

In N13a,b, the improved data allowed the determination of the stellar mass scale, allowing one to produce a more physically consistent analysis, reducing the degeneracies among stellar and dark mass, and taking into account the BCG homogeneity.

The density profiles were calculated by means of the model of DP09 and DP12a described in the previous section. More precisely, the DM density profile can be written as $\rho_{\rm DM}=F(M_{\rm vir},f_{\rm B},j)$ (see Figs. 1a-c in DP12a). The virial mass, $M_{\rm vir}$, or more precisely M_{200}, was obtained by N13a (see also Table 1, second column), and the baryonic fraction, $f_{\rm B}$, was obtained following Giodini et al. (2009), after converting the mass M_{200} of the clusters, given in Table 1 to M_{500} (third column of Table 1). The average errors for the quantities in Table 1, are the following: 0.09 for $\log\frac{M_{200}}{M_\odot}$; 0.012 for $f_{\rm B}$; 0.21 for $\alpha^{\rm N13b}_{\rm gNFW}$; 0.11 for $\alpha^{\rm our}_{\rm gNFW}$; 0.43 for $\log r(\rm core)^{\rm N13b}_{\rm cNFW}$;

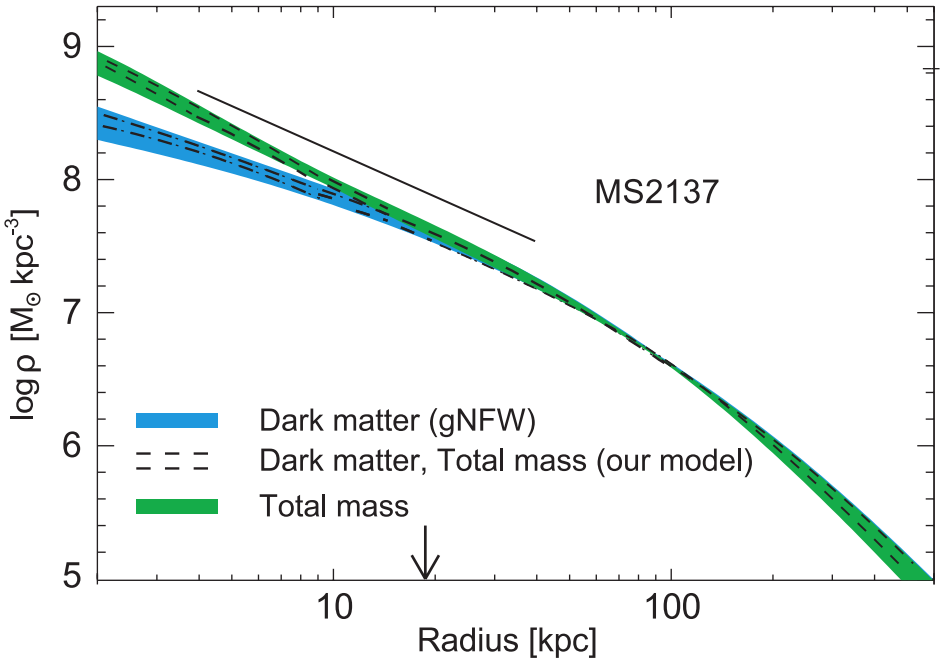

Fig. 1. Density profile of the total mass and DM for MS2137. The blue and green bands represent the DM and the total mass density profiles determined by N13b. The band in black dotted lines is the DM density profile obtained in this paper. The band widths represent the 1σ uncertainty. The bottom arrow is the three-dimensional half-light radius of the BCG. The segment with the slope $r^{-1.13}$ spans the radial range $r = 0.003 - 0.03 r_{200}$.

0.22 for $\log r(\mathrm{core})^{\mathrm{our}}_{\mathrm{cNFW}}$; 0.59 for $\frac{M_{\mathrm{BCG}}}{10^{11} M_{\odot}}$ and 0.29 for $\frac{M_{\mathrm{BCG}}}{10^{11} M_{\odot}}$.

The shape of the density profile also depends on the angular momentum of the cluster. In the case of clusters of galaxies, differently from the case of galaxies, the role of the "ordered" angular momentum is not so important, since clusters have very small rotational velocity, while the "random" angular momentum, j, is significant (see DP12a). As in DP09, for the reason now quoted, we assumed the same "ordered" angular momentum for the clusters studied, fixing it in terms of the spin parameter $\lambda = 0.03$, a typical value obtained by Gottlöber & Yepes (2007). The "random" angular momentum j was considered as a free parameter and fixed by fitting the final DM density profile, similarly to DP12a for the clusters A611, A383, MACS J1423 and RXJ1133, and in DP12b for dwarf galaxies. In other words, knowing M_{vir}, and f_{B}, we adjusted the value of j, so that $\rho_{\mathrm{DM}} = F(M_{\mathrm{vir}}, f_{\mathrm{B}}, j)$ reproduces the observed clusters profiles, through a maximum likelihood analysis. The values of the "random" angular momentum, so obtained, were expressed in terms of j_*[4], and are reported in Table 1 (last column).

In Fig. 1 we show an example of the radial density profiles for the DM halo of MS2137 calculated with the model of N12b and the model of this paper. The

[4] j_* is the "random" angular momentum reproducing the result of DP09 (Fig. 5), and similarly the thick solid line in DP12a (Fig. 1a-c).

blue and green bands represent the density profile of DM and the total density profile with 1σ uncertainties calculated by N13b. The dashed bands represent the DM density profiles obtained with the model of the present paper, and the line segment, having slope $\rho \propto r^{-1.135}$, represents the radius $r = 0.003 - 0.03 r_{200}$. The bottom arrows are the three-dimensional half-light radius of the BCG. The total density profile in the model of this paper matches that observed by N13b (green line) equally well as the DM density profile in the present paper (dashed lines) matches the N13b DM density profile (blue line). Note that in DP09 (Fig. 5), it was shown that the total density profile agrees with a NFW profile.

Fig. 1 shows that the density profile flattens in the inner region of the cluster where the BCG mass starts to be comparable or larger than the DM mass, and this happens in the inner $\simeq 5-10$ kpc (see N13a Fig. 3). At this radii, the total density profile starts to be steeper than the DM density profile, due to increase of the role of the baryon mass (mainly the BCG mass) at these radii. At radii $\geq 5 - 10$ kpc the total density profile and the DM profile are very close, since DM is dominating on the baryon component. Outside the inner region of the clusters the slope of the total density profiles (and also DM) are comparable in different clusters. At these radii the total mass density profile is in agreement with the NFW profile. At radii ≤ 30 kpc, the total density profile is close to the NFW profile, and as observed by N13b this somehow implies a "tight coordination" among star distribution and the inner DM profile (see the following). Since the total mass (composed by the sum of the DM and the baryonic matter) is well described by the NFW profile in the quoted inner regions of the cluster, and since the baryonic component is dominant in the 5-10 kpc central region, it is logical to expect that the DM density profile is flatter than the NFW one. In fact, as shown by Fig. 1, the inner DM profiles are shallower than the NFW profile ($\alpha < 1$), and at the same time a scatter is seen in the inner slope between clusters.

This is better shown in Figs. 2a-b, plotting the slope of the inner profile, α, and the core radius, $r_{\rm core}$, versus the BCG effective radius $R_{\rm e}$, which is the radius containing half of the light[6]. The slope α and the core radius were obtained by parameterizing the halo as a generalized NFW model (gNFW), and as a cored NFW model (cNFW), respectively. Note that, as already stressed by N13b, the choice of the two different parameterizations (gNFW or cNFW) does not affect the result. The values of α and $r_{\rm core}$ obtained by N13b are given in Table 1 (columns 4 and 6), and the values of the same parameters obtained in the model of this paper are given in in columns 5 and 7 of the same table.

In Fig. 2a we reproduce Fig. 5 from N13b, and in Fig. 2b we plot the same quantities obtained using the model of this paper. The gray points in the upper

[5] This is the average slope of the cluster dissipationless CDM simulations in the Phoenix project (Gao et al. 2012).

[6] The gNFW is given by

$$\rho_{\rm DM}(r) = \frac{\rho_s}{(r/r_s)^{\alpha}(1 + r/r_s)^{(3-\alpha)}} \tag{9}$$

which has a central cusp with $d\log\rho_{\rm DM}/d\log r \to 0$. The cored NFW (cNFW) model is given by

$$\rho_{\rm DM}(r) = \frac{b\rho_s}{(1 + br/r_s)(1 + r/r_s)^2} \tag{10}$$

and has a central density core within r_s/b. Both the gNFW, and the cNFW profiles reduce to a NFW profile for $\alpha = 1$, and $r_{\rm core} \to 0$.

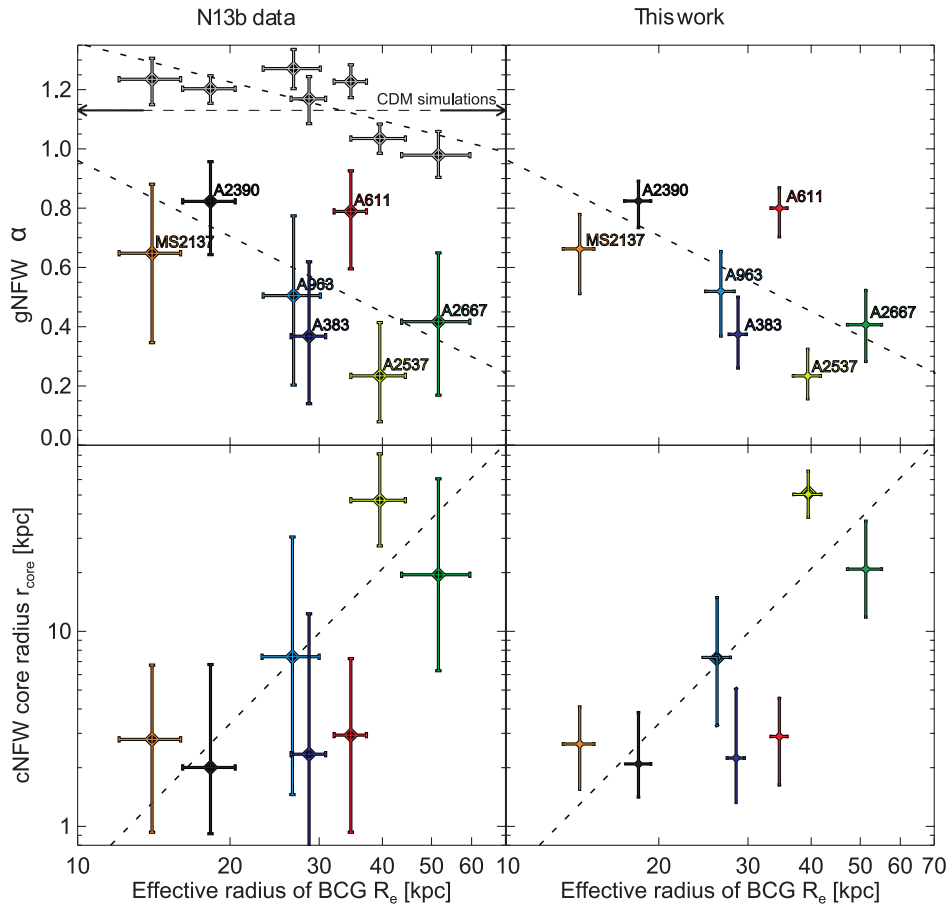

Fig. 2. Correlation among the inner DM profile and the BCG size. Top left panel: gray points (region with $\alpha > 0.9$) represent the total density profile presented in N13a, and the dashed horizontal line represents the mean slope in Gao et al. (2012) CDM-only simulations. The colored points are the β vs. R_e values for the clusters obtained using the gNFW by N13b. The dotted lines are the least-square fits. Bottom left panel: the core radii, $r_{\rm core}$ of the cNFW model vs. $R_{\rm e}$. Top and bottom right panels: the same as the left panels but giving the results obtained by means of the model of this paper.

part of Fig. 2a, taken from N13b, represent the total density profile presented in N13a, and the dashed horizontal line represents the mean slope in Gao et al. (2012) CDM-only simulations. The dotted line shows a weak slope change from one cluster to another. The colored points with error bars show that in real clusters the previous scatter is much larger: clusters having larger BCGs have a shallower inner slope, with respect to clusters having larger BCGs. Similarly, clusters having smaller BGCs have smaller core radii (see the bottom panel). The dotted lines are least-square linear fits to the data. The previous correlation (larger BCG having flatter density DM profiles) is in line with what was previously written. A larger BCG has a larger total mass, and then the DM mass, $M_{\rm DM} = M_{\rm total} - M_{\rm baryon}$, in the inner regions is less than in a smaller BCG, and consequently the inner DM

slope is smaller. The "constraint" that the total mass has a density profile with $\alpha \simeq 1$, suggests that the inner profile shape and slope is strictly connected to star formation in the inner part of the cluster.

The comparison of Figs. 2a and 2b shows that the slopes obtained with the model of this paper are very close to those given by observations. The result of the model shows the same correlations among α, $r_{\rm core}$ and $R_{\rm e}$ as observations. The Spearman rank correlation coefficient and the corresponding P-value relative to α and $r_{\rm core}$ obtained from the model of this paper, are close to those obtained by N13b. In the case of the α vs. R_e correlation, we have $\rho = -0.58$, $P = 0.2$ (N13b obtained $\rho = -0.57$, $P = 0.18$), while for the correlation $r_{\rm core}$ vs. $R_{\rm e}$ we have $\rho = +0.72$, $P = 0.07$ (N13b obtained $\rho = +0.71$, $P = 0.07$). we should note that the density profile was obtained using the "random" angular momentum, j, as a free fitting parameter. Then the theoretical density profile was obtained by fitting the model profile with the observed density profile. In these conditions one should expect that if the observed clusters have correlations among some quantities, these will appear in the model, as observed in Fig. 2.

4. DISCUSSION

The correlations shown in Fig. 2, and the scatter from cluster to cluster can be explained according to the model of this paper (DP09, DP12a) as follows. At high z, the proto-structure containing gas and DM, is in its linear phase. In the SIM, the proto-structure is divided into shells, which initially expand with Hubble flow until the maximum radius and then collapse. The DM mass component collapses before the baryonic mass component, and baryons fall in the DM potential wells, radiating part of their energy and forming clumps which condense into stars (see Li et al. (2010) (Sect. 2.2.2, 2.2.3), De Lucia & Helmi 2008). In the baryon collapse phase, DM is compressed in the so-called "adiabatic contraction" (AC) (Blumenthal et al. 1986; Gnedin et al. 2004, 2011), and the star formation begins. This dissipational process, happening at $z \geq 2$ (see DP09, Figs. 3 and 5) gives rise to a steep density profile, which constitutes the main structure of the BCG (see also Immeli et al. 2004; Lackner & Ostriker 2010), having the scale radius, $R_e \simeq 30$ kpc, which is similar to the sizes of massive galaxies at high redshift (Trujillo et al. 2006; Williams et al. 2010; Newman et al. 2012). Subsequent merging of satellites with the proto-BCG adds stars to the outer parts of the BCG (e.g., Naab et al. 2009; Laporte et al. 2012).

The clumps, formed in the baryon collapse phase, moving to the center are exposed to the DF from DM particles. The result is a motion of the DM towards the outer parts of the proto-structure reducing the central DM density (El-Zant 2001, 2004; DP09; Cole et al. 2011). Other mechanisms proposed to flatten the DM profile are feedback from AGN (e.g. Martizzi et al. 2012).

In the scenario of this paper, one expects the flattening of the DM density profile, and at the same time the anti-correlation of the inner DM slope, α, with the central baryonic content of the cluster (DP09; DP12a). The flattening of the inner slope is due to the fact that the shells in a proto-structure with a larger angular momentum tend to remain closer to the maximum radius, consequently, they do not contribute to the central density. The last column in Table 1 shows

for each cluster the angular momentum j[7]. For example, A2537 and A2667 have a similar value of the virial mass (more correctly M_{200}) and the baryon fraction, f_B. The shallower profile of A2537 is due to its larger j (2.1 $j*$ versus $1.6 j_*$ for A2667)[8].

The dependence of the slope α on the baryonic mass of the whole cluster, and on the mass contained in the inner 10 kpc, was one of the predictions of DP12a (see Figs. 2 and 4b of the quoted paper). The flattening of the profile for larger angular momentum was also found by several authors (Avila-Reese et al. 1998; Hiotelis 2002; Le Delliou & Henriksen 2003; Ascasibar et al. 2004; Williams et al. 2004).

The tendency to have flatter profiles for clusters containing larger quantity of baryons, especially at the center, is due to the fact that the larger is the baryonic content of the cluster the larger is the angular momentum transferred from baryons to DM through DF. This produces the quoted result that DM particles move away from the cluster center.

The profile steepens with mass because of higher density peaks, characterized by larger ν[9], are statistically the forefather of more massive haloes, and the last have a larger central density contrast. Consequently, a generic shell will feel a stronger central potential, and it will expand less than if the same shell was located in a smaller density peak. The final consequence is a lower quantity of angular momentum acquired in the expansion phase giving rise to more concentrated haloes.

The previous discussion pointed out that in the model of this paper the proto-BCG were formed at redshift $z \geq 2$ in the dissipative baryonic collapse, and that the further evolution of the BCG was due to later merging of stars on the BCG (e.g., Naab et al . 2009; Laporte et al. 2012). Subsequently, the satellites infalling in the halo produce a "heating" of DM and flattening of the inner slope (El-Zant et al. 2001, 2004; DP09; Cole et al. 2011).

In this scenario one expects a correlation among the inner mass of the clusters (5 kpc), consisting mainly of stars, and the mass of the core of the cluster (100 kpc), which at the quoted redshift was already formed, and was subsequently subject to little changes (Gao et al. 2004). In Fig. 3, we compare the mass in the central 5 kpc (mainly stars), and that in 100 kpc (mainly DM). The error ellipses (1σ) indicate the uncertainty in the observation results (N13a, left panel) and in the model of this paper (right panel). The correlation with the Pearson coefficient $r = 0.71$ in the model of this paper and $r = 0.70$, two-sided $P = 0.08$ in N13a is found.

The quoted correlation was already discussed in DP12a in the picture of the role of baryons in shaping the DM density profile. It was shown that the baryonic content was of great importance in shaping the density profile, especially the

[7] As we already wrote, the ordered angular momentum is equal for all clusters and has a characteristic spin parameter $\lambda = 0.03$.

[8] For a sake of precision, we should point out that the low value of slope in A2537 could be produced by the fact that it could be a l.o.s. merger (N13a,b). This produces a shallower profile in lensing analysis. At the same time, A2537 is a BCG with the largest mass (the second-largest when looking at the R_e), and according to the previous discussion we expect a shallower profile with respect to other clusters.

[9] $\nu = \delta(0)/\sigma$, where σ is the mass variance, and δ is the fractional density excess in the shell (Del Popolo & Gambera 1996; Del Popolo et al. 2013).

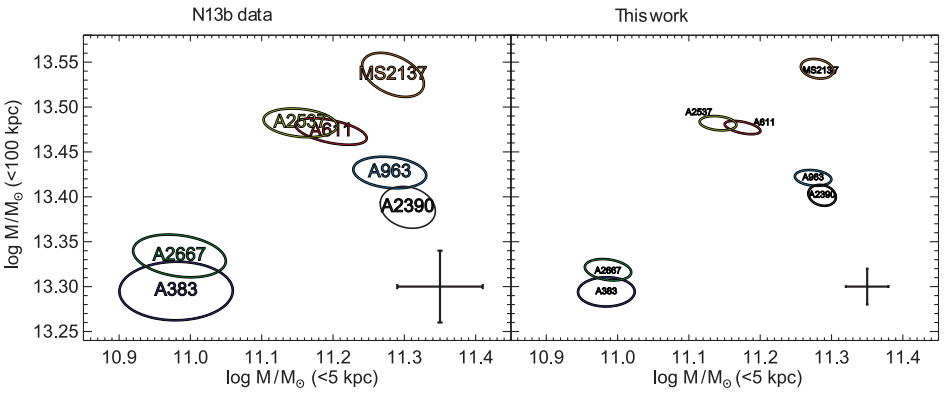

Fig. 3. The mass contained in $r < 100$ kpc vs. the mass within 5 kpc. The error ellipses are for the 1σ uncertainty. The left panel refers to the N13a data and the right panel – to the results of this paper.

baryonic content in the central $\simeq 10$ kpc in the BCG. The cluster final configuration, its star content and its BCG characteristics depend on the initial content of baryons and on the formation process. These considerations lead to think that the BCG mass and the BCG characteristics should be correlated to the baryonic and cluster mass[10]. The previous discussion showed that the DM density profile of the clusters studied has $\alpha < 1$, and that the total density profile is in agreement with the NFW profile.

In the past, observations using lensing (Tyson et al. 1998; Smith et al. 2001; Dahle, Sa02; Gavazzi et al. 2003; Gavazzi 2005; S04; Bradač et al. 2008; Limousin et al. 2008), X-ray (Ettori et al. 2002; Arabadjis, Bautz & Garmire 2002; Lewis, Buote & Stocke 2003), or combination of strong & weak lensing and stellar kinematics (e.g. Sa02; Sa04; Sa08; N09, N11) obtained large scatter in the value of α. In the case of X-ray observations the values of α range from $\alpha = 0.6$ (Ettori et al. 2002) to $\alpha = 1.9$ (Arabadjis et al. 2002). In the case of lensing, Smith et al. (2001) found $\alpha > 1$ for A383, while for the same cluster Sa04 and N11 found $\alpha < 1$ combining the lensing and stellar kinematics. Tyson et al. (1998) found $\alpha = 0.57 \pm 0.024$ for Cl 0024+1654, while Kneib et al. (2003) for the same cluster found $\alpha \simeq 1$. Sa02, Sa04 and Sa08 found a cored profile for MS2137.3-2353, while Gavazzi et al. (2003, 2005) found different results depending on the mass-to-light ratio of the BCG.

The previous discussion shows that a large scatter was also obtained for the inner slope of clusters, and in some cases discrepant results were obtained for the same cluster (see DP12a for a deeper discussion). The quoted scatter and discrepancies have been attributed to (a) degeneracies of α with the concentration parameter, c, or the scale parameter, r_s; (b) spherical modeling of clusters (Morandi et al. 2010); (c) the BCG not taken into account or not properly taken into account; (d) difference in the dynamic range in different studies. Apart of these reasons, the most trivial reason for discrepancies is that many studies do not specify if the study regards to DM or the total density profile; sometimes the inner slope of DM has been compared to that of the total density profile. So,

[10] As shown by Whiley et al. (2008), $M_{\rm BCG} \propto M_{\rm cl}^{0.4}$ or $M_{cl}^{0.5}$ according to the feedback model used, and $M_{\rm BCG} \propto M_{\rm cl}^{0.12\pm0.03}$ for K band magnitudes inside a diameter of 37 kpc.

when comparing different results, particular caution must be beared in mind to the radial range considered, and to understanding if the paper considers the *total* density profile or that of the *dark matter* only. Taking this in account, a comparison of the result of this paper, and those of N13a,b, with more recent observations, usually gives the results in agreement.

In this paper, we are more interested in studying the DM density profiles, so we will make comparisons with previous studies of the DM profile. The results concerning the clusters A963, M2137 and A383 are consistent with those of Sa04, Sa08 and N11. Zappacosta et al. (2006) concluded that for any reasonable mass-to-light ratio, the central regions, where the stellar mass is important, are characterized by a shallower DM profile, in agreement with our previous discussion. Limousin et al. (2008) and Richard et al. (2009) obtained a value of $\alpha_{\rm DM} = 0.92^{+0.05}_{-0.04}$, considering a fit with a gNFW halo and BCG stars. This slope is similar to that of A611 and A2390. X-ray studies of a large sample of clusters by Schmidt & Allen (2007) lead to an estimate of $\alpha_{\rm DM} = 0.88 \pm 0.29$ (95% CL).

So, while the total density profile is in agreement with the NFW profile ($\alpha = 1$), the inner DM profile is shallower than simulations. Even considering recent simulations (Stadel et al. 2009; Navarro et al. 2010) the minimum slope obtained, $\alpha \simeq -0.8$ at 120 pc (Stadel et al. 2009) is larger than the results of observations, and the scatter in the slope from cluster to cluster is much larger than what was found in simulations (Fig. 1, grey points). If some part of the scatter can be explained, as previously reported, in terms of the limits in techniques (e.g., different dynamic ranges in the studies, the BCG role, simplified modeling of clusters), the difference in slope among some clusters is too big to be explained in this way. Since the ΛCDM model predictions at large scale are in agreement with observations, and since the discrepancies among the ΛCDM predictions are seen at scales where astrophysical processes are important, the discrepancy probably is due to the lack of baryons (dominant in the inner part of clusters) in dissipationless simulations, as shown in this paper. This astrophysical solution to the quoted discrepancy is based on the idea that mechanisms "heating" the DM, like the "supernova-AGN-driven flattening" (Navarro et al. 1996; Mashchenko et al. 2006, 2008; Martizzi et al. 2012b), or DF from baryonic clumps (El-Zant et al. 2001, 2004; Romano-Diaz et al. 2008, 2009; DP09; Cole et al. 2011), are able to reduce the inner density[11].

In addition to the astrophysical solution to the problem, other more radical solutions, modifying the particles constituting the DM (e.g., Colin et al. 2000; Sommer-Larsen & Dolgov 2001; Peebles 2000; Kaplinghat et al. 2000; Del Popolo et al. 2013a,b), modifying the power spectrum at small scales (e.g. Zentner & Bullock 2003), considering the modified gravity (e.g., $f(R)$ theory (Buchdal 1970; Starobinsky 1980); $f(T)$ (see Ferraro 2012), and MOND (Milgrom 1983a,b) have been proposed. However, the astrophysical solution is more appealing, since it allows to save the ΛCDM model (see the next section).

[11] Other mechanisms are: interaction of a stellar bar with DM (Weinberg & Katz 2002; McMillan & Dehnen 2005); decay of binary black hole orbits after galaxies merge (Milosavljević & Merritt 2001)

5. CONCLUSIONS

In the present paper we used the model introduced in DP09 to understand what is the role of the baryonic physics in the formation of clusters of galaxies. The main goal of the paper was to understand if the correlations found by N13a,b can be reproduced by means of the improved SIM of DP09. To this aim, we calculated (by means of the quoted model) the DM and total density profiles of the clusters in the following correlations observed by N13a,b (also predicted in DP12a): (a) the correlation between the inner slope of the DM density profile, α, and the effective radius, R_e of the clusters (Fig. 2, top panel); (b) the correlation between the core radius $r_{\rm core}$ and $R_{\rm e}$ (Fig. 2, bottom panel), and (c) the correlation between the mass inside 100 kpc, mainly constituted by DM, and the mass inside 5 kpc, mainly constituted by baryons (Fig. 3), which indicates that the proto-BCG, and the inner cluster halo were already formed in an early stage of evolution, and lately evolved due to accretion.

Using the M_{200} masses of the clusters given in N13a, fixing the baryonic fraction of the clusters following Giodini et al. (2009) and fixing the angular momentum as previously discussed, we obtained the DM and total density profiles of the clusters, which are in good agreement with the N13b observations (see Fig. 1). As already seen in DP12a, the density profiles depend on the baryonic fraction (mainly the central baryonic concentration) and angular momentum. So, if the baryonic content has an important role in forming the final structure of clusters, a fundamental role should be also played in the dynamics of the cluster constituents.

In the inner region, both baryons and DM contribute significantly to the total mass. As seen in Fig. 1, at the radii up to 5–10 kpc, the mass distribution is dominated by stars, while outside these radii all mass is in the form of DM. This result shows the existence of a "tight coordination" among the inner DM and the star distribution, as implied by the fact that the NFW-like profile is not generated by DM or baryons only, but by their mutual contribution. The quoted coordination is further supported by the correlation among the masses within 5 kpc and 100 kpc (Fig. 3), which indicates that the time-scales of formation of the BCG and the inner cluster are similar. As discussed in DP12a, the final configuration of a cluster depends from the baryonic content and the formation process. In a hierarchical model of structure formation, we should expect that the the final inner baryonic content and the BCG mass are correlated with the total baryonic and with the mass of the cluster (see Whiley et al. 2008).

As a further consequence, the inner DM density profile must have a slope $\alpha < 1$, since the total mass is the sum of DM and baryons, and since in the inner 5–10 kpc baryons dominate. This is exactly what we see in Fig. 2, and Table 1: the slope of all clusters is flatter than $\alpha = 1$: the maximum value (including the error) is $\alpha = 0.88$ in the case of A2390 and the minimum $\alpha = 0.14$ in the case of A2537.

Moreover, the quoted figures and Table 1 show a large scatter in the inner slope from one cluster to another, and at the same time (Fig. 2) an anti-correlation between α and R_e: the clusters hosting larger BCGs have flatter slopes. This anti-correlation is due to the fact that in the case when the total mass has NFW-like profile, the clusters having more massive BCG must contain less DM at their centers. This implies that they must have a flatter DM slope. As discussed in DP12a, the quoted scatter is related to the environment. Different baryonic fraction and the angular momentum change the profile of the structure, namely, larger baryon content and larger angular momentum give rise to flatter inner slopes.

The density profile shapes of the clusters studied and the correlations found by N13a,b all are well described in the model of the present paper (DP09, DP12a). The physical picture of the cluster formation is characterized, in agreement with the N13a,b conclusions, by an initial dissipative phase giving rise to a steep stellar density profile, followed by the flattening of the DM density profile due to the heating of DM by baryonic clumps collapsing to the cluster center.

REFERENCES

Allen S. W., Evrard A. E., Mantz A. B. 2011, ARA&A, 49, 409
Antonuccio-Delogu V., Colafrancesco S. 1994, ApJ, 427, 72
Arabadjis J. S., Bautz M. W., Garmire G. P. 2002, ApJ, 572, 66
Ascasibar Y., Yepes G., Gottlsober S. 2004, MNRAS, 352, 1109
Astashenok A.V., A. Del Popolo A. 2012, Class. Quant. Grav., 29, 085014
Avila Reese V., Firmani C., Hernandez X. 1998, ApJ, 505, 37
Babyk Iu., Del Popolo A., Vavilova I. 2012c, arXiv:1208.2424
Babyk Iu., Melnyk O., Elyiv A. 2012a, Advances in Astron. & Space Phys., 2, 56
Babyk Iu., Melnyk O., Elyiv A. 2012b, Advances in Astron. & Space Phys., 2, 188
Babyk Iu., Vavilova I. 2014, Ap&SS, 349, 415
Blumenthal G. R., Faber S. M., Flores R., Primack J. R. 1986, ApJ, 301, 27
Bradac M., Schrabback, T., Erben, T. et al. 2008, ApJ, 681, 187
Buchdahl H. A. 1970, MNRAS, 150, 1
Cardone V. F., Del Popolo A., Tortora C., Napolitano N. R. 2011, MNRAS, 416, 1822
Cardone V. F., Sereno M. 2005, A&A, 438, 545
Cardone V. F., Del Popolo A. 2012, MNRAS, 427, 3176
Cole D. R., Dehnen W., Wilkinson M. I. 2011, MNRAS, 416, 1118
Colin P., Avila-Reese V., Valenzuela O. 2000, ApJ, 542, 622
Cremenelli P., D'Amico G., Norena J. et al. 2009, arXiv:0911.2701v2
Dahle H., Hannestad S., Sommer-Larsen J. 2003, ApJ, 588, L73
De Lucia G., Helmi A. 2008, MNRAS, 391, 14
Del Popolo A. 2007, Astron. Rep., 51, 169
Del Popolo A. 2009, ApJ, 698, 2093
Del Popolo A. 2010, MNRAS, 408, 1808
Del Popolo A. 2011, JCAP, 07, 014
Del Popolo A. 2012a, MNRAS, 424, 38
Del Popolo A. 2012b, MNRAS, 419, 971
Del Popolo A. 2013, AIP Conf. Proc., 1548, 2
Del Popolo A. 2014, IJMPD, 23, 1430005
Del Popolo A., Cardone V. F. 2012, MNRAS, 423, 1060
Del Popolo A., Cardone V. F., Belvedere G. 2013, MNRAS, 429, 1080
Del Popolo A., Gambera M. 1996, A&A, 308, 373
Del Popolo A., Gambera M. 1997, A&A, 321, 691
Del Popolo A., Hiotelis N. 2014, JCAP, 01, 047
Del Popolo A., Kroupa P. 2009, A&A, 502, 733
Del Popolo A., Lima J. A. S., Fabris J. C., Rodrigues D. C. 2014, JCAP, 04, 021
Del Popolo A., Pace F., Lima J. 2013a, IJMPD, 22, Is. 8, id. 1350038

Del Popolo A., Pace F., Lima J. 2013b, MNRAS, 430, 628
Del Popolo A., Pace F., Maydanyuk S. P. et al. 2013c, Physical Review D, 87, Is. 4, id. 043527
El-Zant A. A., Shlosman I., Hoffman Y. 2001, ApJ, 560, 636
El-Zant A. A., Hoffman Y., Primack J. et al. 2004, ApJ, 607, L75
Ettori S., Fabian A. C., Allen S. W., Johnstone R. M. 2002, MNRAS, 331, 635
Ferraro R. 2012, AIP Conf. Proc., 1471, 103
Fillmore J. A., Goldreich P. 1984, ApJ, 281, 1
Flores R. A., Primack J. R. 1994, ApJ, 427, L1
Gao L., Loeb A., Peebles P. J. E. et al. 2004, ApJ, 614, 17
Gao L., Navarro J. F., Frenk C. S. et al. 2012, MNRAS, 425, 2169
Gavazzi R. 2005, A&A, 443, 793
Gavazzi R., Fort B., Mellier Y. et al. 2003, A&A, 403, 11
Giodini S., Pierini D., Finoguenov A. et al. 2009, ApJ, 703, 982
Gnedin O. Y., Ceverino D., Gnedin N. Y. et al. 2011, arXiv:1108.5736
Gnedin O. Y., Kravtsov A. V., Klypin A. A., Nagai D. 2004, ApJ, 616, 16
Gottlöber S., Yepes G. 2007, ApJ, 664, 117
Gunn J. E. 1977, ApJ, 218, 592
Gunn J. E., Gott J. R. 1972, ApJ, 176, 1
Gustafsson M., Fairbairn M., Sommer-Larsen J. 2006, Phys. Rev. D, 74, 123–522
Hiotelis N. 2002, A&A, 383, 84
Hiotelis N., Del Popolo A. 2006, Ap&SS, 301, 167
Hiotelis N., Del Popolo A. 2013, MNRAS, 436, 163
Hu W., Kravtsov A. V. 2003, ApJ, 584, 702
Immeli A., Samland M., Gerhard O., Westera P. 2004, A&A, 413, 547
Jullo E., Kneib J.-P., Limousin M. et al. 2007, NJPh, 9, 447
Kaplinghat M., Knox L., Turner M. S. 2000, Phys. Rev. Lett., 85, 3335
Keeton C. R. 2001, ApJ, 561, 46
Klypin A., Zhao H-S., Somerville R.S. 2002, ApJ, 573, 597
Klypin A., Kravtsov A. V., Bullock J. S., Primack J. R. 2001, ApJ, 554, 903
Kneib J.-P., Hudelot P., Ellis R. S. et al. 2003, ApJ, 598, 804
Kneib J.-P., Natarajan P. 2011, A&ARv, 19, 47
Komatsu E., Smith K., Dunkley J. et al. 2011, ApJS, 192, 18
Lackner C. N., Ostriker J. P. 2010, ApJ, 712, 88
Laporte C. F. P., White S. D. M., Naab T. et al. 2012, MNRAS, 424, 747
Le Delliou M., Henriksen R. N. 2003, A&A, 408, 27
Lewis A. D., Buote D. A., Stocke J. T. 2003, ApJ, 586, 135
Li Y-S., De Lucia G., Helmi A. 2010, MNRAS, 401, 2036
Limousin M., Richard J., Kneib J.-P. et al. 2008, A&A, 489, 23
Lukic Z., Reed D., Habib S., Heitmann K. 2009, ApJ, 692, 217
Martin J. 2012, arXiv:1205.3365
Martizzi D., Teyssier R., Moore B., Wentz T. 2012a, MNRAS, 422, 3081
Martizzi D., Teyssier R., Moore B. 2012b, MNRAS, 420, 2859
Mashchenko S., Couchman H. M. P., Wadsley J. 2006, Nature, 442, 539
Mashchenko S., Wadsley J., Couchman H. M. P. 2008, Science, 319, 174
McMillan P. J., Dehnen W. 2005, MNRAS, 363, 1205

Milgrom M. 1983a, ApJ, 270, 365
Milgrom M. 1983b, ApJ, 270, 371
Milosavljevic M., Merritt D. 2001, ApJ, 563, 34
Mo H. J., Mao S., White S. D. M. 1998, MNRAS, 295, 319
Moore B. 1994, Nature, 370, 629
Moore B., Governato F., Quinn T. et al. 1998, ApJ, 499, L5
Morandi A., Pedersen K., Limousin M. 2010, ApJ, 713, 491
Naab T., Johansson P. H., Ostriker J. P. 2009, ApJ, 699, L178
Navarro J. F., Frenk C. S., White S. D. M. 1996, ApJ, 462, 563
Navarro J. F., Frenk C. S., White S. D. M. 1997, ApJ, 490, 493
Navarro J. F., Hayashi E., Power C. et al. 2004, MNRAS, 349, 1039
Navarro J. F., Ludlow A., Springel V. et al. 2010, MNRAS, 402, 21
Newman A. B., Ellis R. S., Bundy K., Treu T. 2012, ApJ, 746, 162
Newman A. B., Treu T., Ellis R. S. et al. 2009, ApJ, 706, 1078
Newman A. B., Treu T., Ellis R. S., Sand D. J. 2011, ApJ, 728, 39
Newman A. B., Treu T., Ellis R. S. et al. 2013a, ApJ, 765, 25
Newman A. B., Treu T., Ellis R. S. et al. 2013b, ApJ, 765, 24
Oh S-H., Brook C., Governato F. et al. 2010, AJ, 142, 24
Peebles P. J. E. 1969, ApJ, 155, 393
Peebles P. J. E. 2000, ApJ, 534, L127
Percival W. J., Reid B., Eisenstein D. et al. 2010, MNRAS, 401, 2148
Pratt G. W., Arnaud M., Pointecouteau E. 2006, A&A, 446, 429
Richard J., Pei L., Limousin M. et al. 2009, A&A, 498, 37
Rix H.-W., de Zeeuw P. T., Cretton N. et al. 1997, ApJ, 488, 702
Romano-Diaz E., Shlosman I., Heller C., Hoffman Y. 2009, ApJ, 702, 1250
Romano-Diaz E., Shlosman I., Hoffman Y., Heller C. 2008, ApJ, 685, L105
Ryden B. S. 1988, ApJ, 329, 589
Ryden B. S., Gunn J. E. 1987, ApJ, 318, 15
Sand D. J., Treu T., Ellis R. S. 2002, ApJ, 574, L129
Sand D. J., Treu T., Ellis R. S. et al. 2008, ApJ, 674, 711
Sand D. J., Treu T., Smith G. P., Ellis R. S. 2004, ApJ, 604, 88
Schaefer B. M. 2009, Int. J. Mod. Phys. D, 18, 173
Schmidt R. W., Allen S. W. 2007, MNRAS, 379, 209
Smith G. P., Kneib J., Ebeling H. et al. 2001, ApJ, 552, 493
Sommer-Larsen J., Dolgov A. 2001, ApJ, 551, 608
Stadel J., Potter D., Moore B. et al. 2009, MNRAS, 398, 21
Starobinsky A. A. 1980, Physics Letters B, 91, 99
Treu T., Koopmans L. V. E. 2002, ApJ, 575, 87
Trujillo I., Forster S. N., Rudnick G. et al. 2006, ApJ, 650, 18
Tyson J. A., Kochanski G. P., dell'Antonio I. P. 1998, ApJ, 498, L107
Weinberg S. 1989, Rev. Mod. Phys., 61, 1
Weinberg M. D., Katz N. 2002, ApJ, 580, 627
Whiley I. M., Aragon-Salamanca A., De Lucia G. et al. 2008, MNRAS, 387, 1253
White M. 2001, A&A, 367, 27
Williams L. L. R., Babul A., Dalcanton J. J. 2004, ApJ, 604, 18
Williams R. J., Quadri R. F., Franx M. et al. 2010, ApJ, 713, 738

Zappacosta L., Buote D. A., Gastaldello F. et al. 2006, ApJ, 650, 777
Zentner A. R., Bullock J. S. 2003, ApJ, 598, 49